VERSITA

Acta Geophysica
vol. 56, no. 1, pp. 114-141
DOI: 10.2478/s11600-007-0040-4

# Effects of wind shear on the atmospheric convective boundary layer structure and evolution

Evgeni FEDOROVICH[1] and Robert CONZEMIUS[1,2]

[1]School of Meteorology, University of Oklahoma, Norman, Oklahoma, USA
e-mail: fedorovich@ou.edu

[2]WindLogics Inc., Grand Rapids, Minnesota, USA

Abstract

The article reviews past accomplishments and recent advances in conceptual understanding, numerical simulation, and physical interpretation of the wind shear phenomena in the atmospheric convective boundary layer.

**Key words:** convection, wind shear, boundary layer, numerical simulation.

## 1. INTRODUCTION

In this article, past accomplishments and recent advances in conceptual understanding of the wind shear phenomena in the atmospheric convective boundary layer (CBL), originating from observations and numerical simulations, will be reviewed.

The CBL is a particular case of the atmospheric planetary boundary layer – an interfacial region between the free atmosphere and the Earth surface. The subject of our consideration is the dry (or clear) CBL (Holtslag and Duynkerke 1998) which is primarily forced by the buoyancy production at the underlying surface of the Earth. However, a purely buoyancy-driven CBL rarely exists in nature. Usually in addition to the dominant buoyancy forcing, the CBL flow is affected by wind shears which modify both its internal structure and integral behavior to the extent that these effects cannot be generally ignored. To date, many studies of CBL flows have focused on the shear-free CBL which has been reasonably well studied in laboratory conditions, through atmospheric measurements, and by numerical simulations. Far fewer studies have been performed on sheared CBLs, and most of the theories and parameterizations resulting from those studies have not been sufficiently tested over a wide range of external atmospheric conditions associated with sheared CBL cases.

Within the traditional conceptual framework employed in the meteorological studies of the CBL, the boundary layer is considered as a horizontally (quasi-) homogeneous entity, where horizontal averages are taken as substitutes for ensemble averages, and the horizontally averaged flow variables are considered as functions of time and height only. A different perspective is used in the wind tunnel studies of the CBL, where the case of (quasi-)stationary, spatially evolving flow is considered (see, *e.g.*, Fedorovich *et al*. 1996). Adopting the former framework, one may consider three (sub-)layers within the CBL (Stull 1988): the **surface layer** (comprising approximately 10% of the total CBL depth), where the underlying surface inhibits vertical convective motions; the **mixed layer**, often referred to as the main portion of CBL, where mixing by convective motions typically keeps the vertical gradients of meteorological fields relatively small; and **entrainment zone** (or **layer**) at the CBL top, where the vertical gradients once again become large because of the suppression of vertical mixing by stable stratification. In each of these layers, the meteorological quantities are regarded horizontally averaged. Above the CBL is the stably stratified free atmosphere.

Among diverse physical processes that determine the CBL evolution, the principal one is convective **entrainment**, the process by which more buoyant air from the free atmosphere is engulfed by the CBL air and, as a result, becomes part of the CBL air (Randall and Schubert 2004). Among other important processes that control CBL development, in conjunction with entrainment, are horizontal divergence/convergence of the CBL flow (Stull 1988, Fedorovich and Thäter 2001) associated with subsidence/lifting at the CBL top, and differential temperature advection, which is a manifestation of baroclinicity of the CBL flow (Sorbjan 2004).

Atmospheric experiments, laboratory models, and numerical methods constitute a triad of approaches used to investigate the structure and evolution of the CBL under conditions of significant wind shear. Atmospheric data come from balloon-borne vertical soundings, near-surface measurements, and aircraft, tethersonde, and radar observations (Lenschow 1970, 1974, Lemone 1973, Pennel and Lemone 1974, Hoxit 1974, Arya and Wyngaard 1975, Mahrt and Lenschow 1976, Kaimal *et al*. 1976, Stull 1976a, b, c, Zeman and Tennekes 1977, Caughey and Palmer 1979, Lenschow *et al*. 1980, Tennekes and Driedonks 1981, Driedonks 1982, Garratt and Wyngaard 1982, Brost *et al*. 1982a, b, Boers *et al*. 1984, Chou *et al*. 1986, Batchvarova and Gryning 1991, Grossman 1992, Betts *et al*. 1992, Betts and Ball 1994, Batchvarova and Gryning 1994, Betts and Barr 1996, Barr and Strong 1996, Davis *et al*. 1997, Flamant *et al*. 1997, Lemone *et al*. 1999, Angevine 1999, Schneider and Lilly 1999, Angevine *et al.* 2001, Pino *et al*. 2003, and Margulis and Entekhabi 2004). See Conzemius and Fedorovich (2006a) for a more detailed overview of these studies.

Two main difficulties undermine the utility of atmospheric data for the quantification of shear effects in the CBL: (*i*) the near impossibility of isolating the influence of shear from the effects of other processes determining the CBL structure and (*ii*) insufficient length of atmospheric data samples and time series for a reliable evaluation

of momentum, heat, and turbulence kinetic energy (TKE) budgets. Observational studies of shear effects in atmospheric CBLs are reviewed in Section 2 of this paper.

Laboratory studies of a horizontally evolving sheared CBL conducted by Fedorovich *et al*. (1996, 2001a, b), Fedorovich and Kaiser (1998), and Kaiser and Fedorovich (1998) in the stratified wind tunnel of the University of Karlsruhe, Germany, have revealed significant variability of the CBL turbulence structure and modification of the heat flux at the CBL top due to the influence of various types of imposed shear. Those experiments, however, did not allow direct quantification of the effects of shear on the CBL growth due to the modified entrainment since the flow contraction/expansion effects in the wind tunnel CBL flow ultimately dominated the entrainment. We are not aware of experiments in convective water tanks – successfully used to model the shear-free CBL in Deardorff *et al*. (1969) and numerous succeeding studies – designed to investigate the CBL with shear and buoyancy forcings acting simultaneously.

The dynamics of sheared CBLs has been investigated numerically. After Deardorff (1970a) pioneered the use of large eddy simulation (LES; Pope 2000) to study the atmospheric CBL, a number of LES studies have been conducted that focused on a variety of sheared CBL features: turbulence structure (Deardorff 1972; Sykes and Henn 1989; Khanna and Brasseur 1998; Kim and Park 2003), turbulence dynamics (Moeng and Sullivan 1994), velocity field statistics (Brown 1996), turbulence structure of the entrainment layer (Otte and Wyngaard 2001), mean flow evolution (Pino *et al*. 2003), temperature advection and baroclinicity (Sorbjan 2004), reproducibility of sheared CBLs by different LES codes (Fedorovich *et al*. 2004a), and entrainment dynamics (Kim *et al*. 2003, Conzemius and Fedorovich 2006a).

Another popular approach to study CBL and parameterize it in atmospheric models is based on the so-called bulk model concept. The bulk model equations for the CBL are obtained by vertical integration of Reynolds-averaged equations of boundary layer dynamics and thermodynamics over the whole CBL or its individual regions (sublayers), as outlined in Deardorff (1979), Fedorovich and Mironov (1995), and Fedorovich (1998). Over the last several decades, bulk models of the CBL were employed to predict mixing height for air quality applications, to parameterize boundary layer processes in numerical weather prediction, general circulation, and climate models, and – most importantly – to develop a conceptual understanding of processes underlying the evolution of the CBL. The bulk CBL models proposed to-date differ in their degree of complexity in representation of the CBL structure. The simplest bulk model is the zero order model (ZOM; Lilly 1968, Zilitinkevich 1991, and Fedorovich 1995), in which the whole CBL is represented by a single layer (sometimes called the convectively mixed layer) of height-constant buoyancy and velocity. Stull (1976a, b, c), Zeman and Tennekes (1977), Tennekes and Driedonks (1981), Driedonks (1982), Boers *et al*. (1984), Batchvarova and Gryning (1991, 1994), Fedorovich (1995), and Pino *et al*. (2003) used the ZOM framework to derive expressions for integral budgets of momentum and heat and construct entrainment parameterizations for the sheared CBL.

An alternative bulk model type extensively applied in CBL studies is the first order model (FOM) suggested by Betts (1974). In the FOM, a capping inversion layer with linear velocity and buoyancy changes in the vertical is added atop the convectively mixed layer of height-constant buoyancy and velocity. Mahrt and Lenschow (1976), Kim *et al*. (2006), Pino *et al*. (2006), and Conzemius and Fedorovich (2007) employed the FOM approach in their studies of sheared CBLs. Sorbjan (2004) proposed a parameterization of entrainment in sheared baroclinic CBLs that requires at least a first-order representation of the meteorological profiles throughout the entrainment zone. Conzemius and Fedorovich (2006b) tested and analyzed the capabilities of the zero-order and first-order bulk models, which have been proposed to-date, to predict the entrainment flux in sheared CBLs.

In the present review, the emphasis will be placed on the knowledge about sheared CBLs gained primarily from LES studies since those are the main sources of our current understanding of the structure and dynamics of the considered atmospheric boundary layer type. A review of LES results will constitute the scope of Section 3. Data from LES of the barotropic, equivalent-barotropic, and baroclinic CBL cases will be discussed, and shear effects associated with each of these CBL types will be analyzed. Finally in Section 4, the modern conceptual understanding of the role that wind shears play in modification of the CBL structure and evolution will be overviewed.

## 2. OBSERVATIONAL STUDIES OF SHEARED ATMOSPHERIC CBL

Some of the earliest observational studies of the atmospheric CBL were already dealing with effects of wind shear on the development of the CBL and turbulence structure within it. Lenschow (1970) studied the CBL turbulence structure and TKE budgets and identified shear production of turbulence in the surface layer. Lemone (1973) investigated the structure of CBL rolls using aircraft and instrumented tower data. Pennell and Lemone (1974) extended these studies into experimental analyses of turbulence structure and vertical profiles of the components of the TKE budget in a trade wind boundary layer, finding significant input by shear throughout the CBL below cloud base. Lenschow (1974) looked further into the TKE budgets affected by surface wind shears and developed a model for the CBL depth variation under the influence of shear. These studies provided some quantification of the shear generation of TKE in the surface layer but not at the CBL top. Nonetheless, the performed analyses indicated a significant shear contribution to the TKE budget in the lower CBL for rather typical atmospheric wind speeds on the order of 10 m $s^{-1}$. The obtained estimates of dissipation, however, showed that most of the shear generation near the surface was probably balanced by dissipation. Measurements at the CBL top in the considered studies were not sufficient to address shear generation of TKE in the entrainment zone.

Some evidence for shear effects on CBL structure has been documented with radiosonde data. Hoxit (1974) conducted a study analyzing radiosonde data over four consecutive cold seasons (November through March), finding evidence for a down-

ward turbulent transport of horizontal momentum associated with the vertical shear of the geostrophic wind. The velocity profiles were found to be dependent on the orientation of the thermal wind vector (shear in the geostrophic wind) relative to the surface geostrophic wind vector. The collected data were not presented in a format that would allow the boundary layer top to be precisely identified, but the vertical profiles pointed to the mixing of momentum in a turbulent boundary layer between morning and evening hours. Arya and Wyngaard (1975) developed a physical model of the sheared baroclinic CBL and used it to predict wind profiles in the CBL. The predicted profiles agreed reasonably well with profiles from atmospheric measurements. Kaimal *et al*. (1976) analyzed data from a field experiment in northwestern Minnesota and found unexpectedly large turbulent stress in the upper portion of the CBL, which was taken as evidence of heat and momentum entrainment into the CBL. The data in the upper 40% of the CBL were fairly sparse, so the entrainment fluxes had to be inferred from extrapolation of the lower level measurements. In order to better estimate turbulent fluxes in the upper CBL, an experiment at Ashchurch, Worcestershire, was conducted a couple years later, and the data, presented by Caughey and Palmer (1979), complemented the Minnesota data fairly well, confirming the effects of entrainment revealed by heat and momentum flux profiles in the CBL. Some entrainment flux ratios higher than the shear-free predictions of 0.2 were observed, indicating a possible enhancement of entrainment beyond what would theoretically be found in a shear-free case. Unfortunately, there was some uncertainty in the estimate of the entrainment flux ratio since the surface heat flux was not directly measured (however, it could be inferred by extrapolating the mixed layer heat flux profile to the surface). The considered studies were focused on the second moments of turbulence and did not present much data on mean wind profiles which would have been helpful in relating the entrainment of momentum and heat to shear in the CBL.

Price *et al*. (1978) performed a study of oceanic mixed layer deepening, with the intention of finding a relevant velocity scale for shear-induced mixed layer deepening. Their data indicated that the observed deepening rate scaled best with velocity change across the bottom of the mixed layer. This result has particular relevance to the quantification of the relative contributions of surface and entrainment zone shear to modification of the CBL structure and entrainment.

Observational studies of the CBL in the 1980s provided evidence (though, without or with very little formal quantification) of the enhancement of entrainment by shear. Lenschow *et al*. (1980) analyzed the mean field and second order turbulence statistics budgets in a baroclinic CBL. They discovered strong effects of the larger-scale horizontal temperature gradients in the mean momentum and temperature budgets, but only little influence of those on the second moments of turbulence. Garratt and Wyngaard (1982) analyzed data from three atmospheric experiments and conducted an analysis of wind profiles similar to that of Hoxit (1974), observing strong effects of entrainment on the profiles which, in many instances, were not indicative of profound vertical mixing of momentum in the sheared CBL. The latter finding was supported in a later study by Lemone *et al*. (1999), who observed significantly non-mixed momen-

tum profiles in the CBL when rapid entrainment occurred on a day with strong winds. Brost *et al*. (1982a,b) studied marine, stratocumulus-topped CBLs, some of which developed in the presence of strong wind shears. With shear magnitudes in both the measured and geostrophic winds on the order of 0.01 $s^{-1}$, they found substantial shear production of TKE at the top of the CBL. Boers *et al*. (1984) used six atmospheric case studies of daytime CBL growth from sunrise to quantify effects of shear on the entrainment rate. Batchvarova and Gryning (1991) employed a tethersonde (temperature and humidity sensors tied to a retractable balloon) to measure the CBL temperature profile and to estimate its depth for seven atmospheric CBL growth cases. They evaluated effects of surface shear on the CBL development in terms of friction velocity retrieved from sonic anemometer data. However, their strongest sheared CBL case only had surface winds of about 5 m $s^{-1}$. Chou *et al*. (1986) measured the turbulence in a horizontally evolving CBL during a cold air outbreak over the Atlantic Ocean off the east coast of the United States. Their analysis of the TKE budgets derived from the aircraft data showed that shear was a significant term in the turbulence production in the CBL, not only near the surface, where it was largest, but at the CBL top as well. However, there were only two points in the momentum profile, and the authors acknowledged some uncertainty in the estimate of the local shear at the CBL top since the vertical spacing of flight legs was large. Nevertheless, the data provided evidence that shear production was a significant contributor to the TKE production in that particular CBL.

The First International Satellite Land Surface Climatology Project Field Experiment that took place in 1987 provided plenty of data for the estimation of entrainment flux ratios in sheared CBLs (Grossman 1992, Betts *et al*. 1992, Betts and Ball 1994, Betts and Barr 1996, Margulis and Entekhabi 2004). In most of those studies, some rather large entrainment flux ratios were observed, suggesting that shear enhancement of entrainment might have occurred during the experiment. However, the direct correlation between shear and entrainment flux ratios was relatively weak overall, indicating that factors other than the shear itself (*e.g*., buoyancy and stratification) contributed to the enhancement of entrainment at least to the same extent as wind shears. Barr and Strong (1996) used heat budget methods to analyze data from soundings released from Kenaston and Saskatoon, Canada, in June and July 1991 and found relatively large entrainment flux ratios on the order of 0.5 (the commonly accepted value for the shear-free entrainment is 0.2). Similar methodology was used by Angevine (1999), who also found some rather high entrainment flux ratios in the sheared CBL, where larger entrainment ratio values corresponded to smaller values of the entrainment-zone Richardson number. Davis *et al*. (1997) associated high entrainment flux ratios in CBL with large velocity jumps across the entrainment zone in their field study of CBL over a boreal forest.

Flamant *et al*. (1997) measured the CBL depth and entrainment zone thickness south of the Pyrenees with an aircraft-mounted, downward-looking lidar and made turbulent heat flux measurements at three levels in the CBL using aircraft-mounted sensors. Assuming a linear heat flux profile from the surface to the CBL top, the three-

point heat flux profile was extrapolated to the lidar-estimated height of the CBL top. With this extrapolation, the surface heat flux and the entrainment zone heat flux were estimated. They found the entrainment flux ratio varied from 0.1 in shear-free conditions to about 0.3 when the entrainment zone shear was stronger. Since it is not known exactly how the CBL top, retrieved from lidar data, compares to the level of the heat flux minimum traditionally taken as the CBL top, and because of the fact that most estimates of the entrainment parameters and surface heat flux were extrapolated from measurements within the CBL, the actual values of the entrainment flux ratio might have considerable error. The authors of *op. cit.* were sure, nevertheless, that their experimental results provided clear support for the entrainment enhancement by shear. Plotting their entrainment flux ratios as functions of entrainment zone velocity jumps, however, does not reveal an obvious association between shear and entrainment flux ratio. Angevine *et al*. (2001) analyzed observations of the morning development of the CBL during a series of field campaigns in different geographical locations, including a field experiment at the Cabauw tower in the Netherlands. Wind and temperature readings at several heights up to 200 meters on the tower were used along with surface heat flux measurements. In addition, a 1290-MHz radar profiler was used to detect the onset of turbulence at 200 meters above ground level. These combined measurements showed that heat flux of entrainment may constitute a considerable fraction of the surface heat flux during the morning transition. It was concluded that shear-generated TKE was an apparent cause of relatively strong downward heat flux observed during the morning transition. The experimental data of Angevine (1999) and Angevine *et al*. (2001) provide the most solid atmospheric evidence of enhancement of the CBL entrainment by wind shears.

## 3. LES OF ATMOSPHERIC CBL WITH WIND SHEARS

Most of the LES studies of the dry CBL carried out to date have concentrated on the effects of the principal CBL forcing, which is the convective heat transfer from the warm, underlying surface. Only a few studies have investigated, with the same degree of detail, the effects produced by additional non-buoyant forcings that contribute to the CBL turbulence regime. Wind shear across the CBL is an example of such an external non-buoyant forcing. In LES of sheared CBLs, the shear forcing is introduced through prescribing components of the background (initial) flow field. In simulations of the atmospheric CBL, this initial wind field is either set in geostrophic balance (constant or varying with height) or allowed to have an ageostrophic component as well (Pino *et al*. 2003, Sorbjan 2004, Fedorovich *et al*. 2004a, Conzemius and Fedorovich 2006a). With either setting, horizontal flow velocity field in the free atmosphere far above the CBL is assumed to be in geostrophic balance.

In the case of height-constant geostrophic wind, which is the **barotropic CBL** case, wind shear is initially concentrated in the near-surface portion of the layer where vertical gradients of the flow components result from no-slip conditions at the surface. As the CBL evolves and the vertical mixing of momentum is maintained throughout

the main portion of the CBL, the surface drag leads to an overall decrease of momentum in the CBL and the development of a secondary shear region at the CBL top (Moeng and Sullivan 1994, Conzemius and Fedorovich 2006a). The barotropic CBL is a rather special CBL case. In a more general case of the **baroclinic CBL**, the geostrophic wind components $u_g$ ($x$-component) and $v_g$ ($y$-component) vary with height, and their vertical gradients may be approximately expressed in terms of horizontal changes of the potential temperature $\Theta$ as in Sorbjan (2004):

$$\partial u_g / \partial z = -(\beta / f)\,(\partial \Theta / \partial y)\,, \quad \partial v_g / \partial z = -(\beta / f)\,(\partial \Theta / \partial x)\,,$$

where $\beta = g / \Theta_0$ is the buoyancy parameter ($g$ is the gravitational acceleration, $\Theta_0$ = const is the reference temperature), and $f$ is the Coriolis parameter. If only one component of the geostrophic wind is assumed to change with height, while the other one is taken zero, there will be no geostrophic advection of heat (potential temperature) in the direction represented by the latter component. This special case of the so-called **equivalent barotropic** CBL was the subject of several LES studies starting with Brown (1996). Sorbjan (2004) was apparently the first to accurately incorporate the temperature advection as a baroclinicity feature in the LES framework for the sheared atmospheric CBL.

### 3.1 Barotropic CBL

Moeng and Sullivan (1994) numerically investigated two barotropic CBL cases with relatively large contributions of (surface) shear to the CBL dynamics. They observed a reorganization of the turbulence structure of CBL as the relative contribution of shear to the turbulence production increased. Under conditions of slight buoyancy and strong shear, the irregular polygonal updraft/downdraft structures (cells) characteristic of the shear-free CBL was replaced by a series of roll-like structures especially visible in the center of the layer. Those rolls were rather similar to the structures observed by Lemone (1973) in the atmospheric CBL under analogous conditions.

The results of Moeng and Sullivan (1994) supported the previous analysis of Holtslag and Nieuwstadt (1986) and the LES findings of Sykes and Henn (1989), who had identified the ratio of the friction velocity to the Deardorff (1970b) convective velocity, $u_* / w_*$, as a parameter that controls the cells-to-rolls transition in the CBL flow. Another parameter used to relate shear and buoyancy forcings in the CBL is the ratio of the Monin–Obukhov length scale $L$ to the CBL depth scale $z_i$ connected to $u_* / w_*$ as $-L / z_i = (u_* / w_*)^3 / k$, where $k = 0.4$ is the von Kármán constant.

With very small $u_* / w_*$ values, the structure of CBL flow is essentially cellular. With increasing $u_* / w_*$, rolls start to form in the CBL, and the turbulence structure of the layer becomes qualitatively distinctively different from that of the shear-free CBL. The turbulence statistics, which are a more quantitative measure, change correspondingly. The specific value of $u_* / w_*$ that separates the regimes of shear-free and sheared convection apparently depends on particular features of the analyzed CBL flow.

According to Holtslag and Nieuwstadt (1986), this threshold $u_*/w_*$ value is about 0.35. In the CBL simulated by Moeng and Sullivan (1994), the transitional value of $u_*/w_*$ was about 0.65 ($-L/z_i \sim 0.69$), apparently due to the joint effect of strong capping inversion and Coriolis force.

In a comprehensive LES study of the three-dimensional structure of buoyancy- and shear-induced turbulence in the atmospheric boundary layer, Khanna and Brasseur (1998) spanned a vast range of CBL cases starting from a nearly shear-free CBL ($-L/z_i = 0.0014$, $u_*/w_* = 0.082$) to an essentially shear-driven boundary layer ($-L/z_i = 2.3$, $u_*/w_* = 0.97$). This study supported earlier findings by Moeng and Sullivan (1994) regarding the modification of the CBL turbulence structure by surface wind shear and provided additional insights into the individual properties of convective thermals and rolls. An interaction between outer eddies that scale with the CBL depth and near-ground streaks has been identified, with a tendency towards strengthening at larger $u_*/w_*$. It was concluded that the shear-dominated structure of the unstable near-surface flow region directly influences the global structure of the sheared CBL.

Kim *et al*. (2003) performed an LES study examining the effects of Kelvin–Helmholtz (K-H) type instabilities at the top of the CBL under strong wind conditions, examining the shear-driven processes that might enhance CBL entrainment. They found that the K-H instabilities developed along the top of horizontal CBL rolls as the Richardson number approached the critical value of 0.25 for the onset of K-H instability. They also concluded that any theory of entrainment must take into account the shear across the CBL top since the considered studies were conducted under atmospheric conditions rather typical with respect to wind speeds and shear. Their study made a rather thorough analysis of the entrainment mechanism at the CBL top but did not quantify what the shear enhancement might be or what the relative effects of surface shear *versus* entrainment zone shear might be.

Pino *et al*. (2003) looked at the effects of shear on the entrainment rate in three CBL evolution cases using LES in conjunction with atmospheric data. According to the authors, their primary goal was not to compare each observed profile with the LES results, but to show that the LES could simulate the main characteristics of the observed convective boundary layer when the shear contribution could play a key role. The simulations were initiated with atmospheric temperature profile observed in the morning of the day when CBL evolution was studied. The LES runs were conducted with three initial wind field configurations that corresponded, respectively, to a shear-free CBL case, a case with height-constant wind, and a case with height-dependent wind. The wind profile prescribed for the last of these cases was the closest to the actual wind distribution observed on the simulated day. In the simulation with height-constant wind, the developed CBL was deeper than the shear-free CBL after the same time in the simulation (Fig. 1). The inclusion of surface shear led to the decrease of the buoyancy production term in the TKE budget near the surface and at the inversion level, but it did not noticeably change this production term in the middle of the layer.

As in the LES study of Moeng and Sullivan (1994), with initial wind shear prescribed only at the surface, an elevated shear developed at the inversion level as the CBL grew with time. However, wind shear remained relatively small in the middle of the CBL due to the effective convective mixing throughout the layer. In the presence of surface shear, higher values at greater heights were found for the entrainment fluxes as compared to the shear-free CBL simulation. From that, the authors concluded that surface shear enhances the entrainment flux.

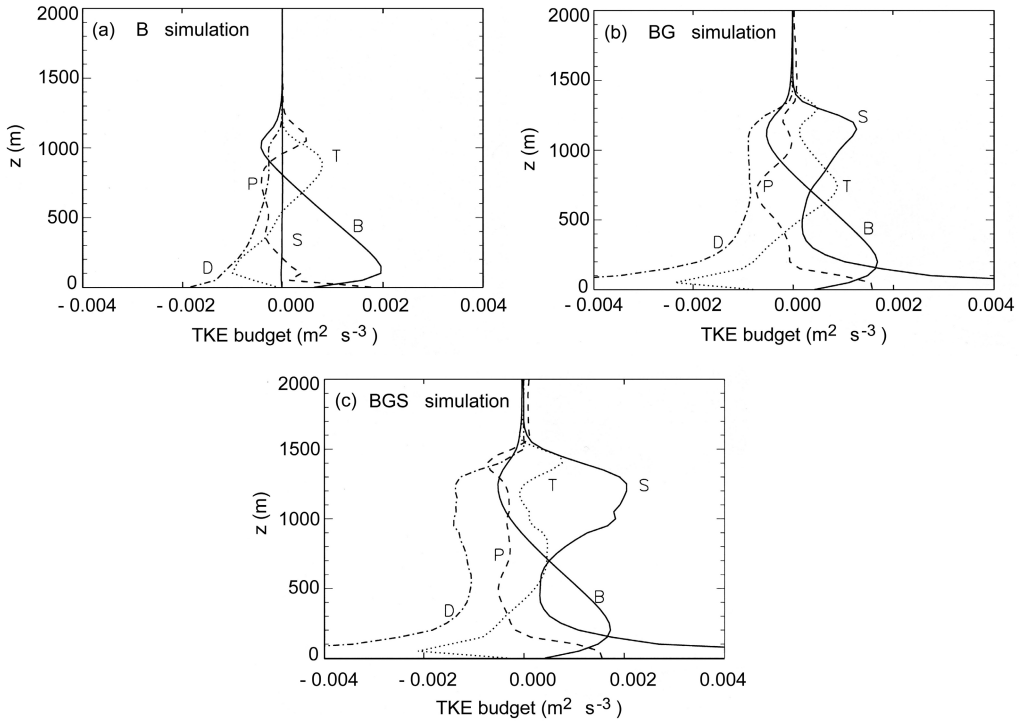


Fig. 1. Vertical profiles of individual terms (buoyancy B, dissipation D, pressure P, transport T, and shear S) of the TKE budget in LES of shear-free CBL (a), CBL with surface shear forcing (b), and CBL with geostrophic shear forcing (c). Profiles represent averages between 7 and 8 h into simulations. From Pino *et al*. (2003).

Conzemius and Fedorovich (2006a) used a modified version of LES code from Fedorovich *et al*. (2001a) to elucidate CBL surface shear effects *versus* the effects of shear across the boundary layer top. A subset of the investigated barotropic CBL cases with a height-constant geostrophic wind, denoted as GC cases in Conzemius and Fedorovich (2006a), all had the initial shear concentrated at the surface. Simulation results for those cases were compared against LES data for shear-free CBL cases, designated as the NS cases. Schematics of CBL cases simulated in Conzemius and Fedorovich (2006a) are shown in Fig. 2.

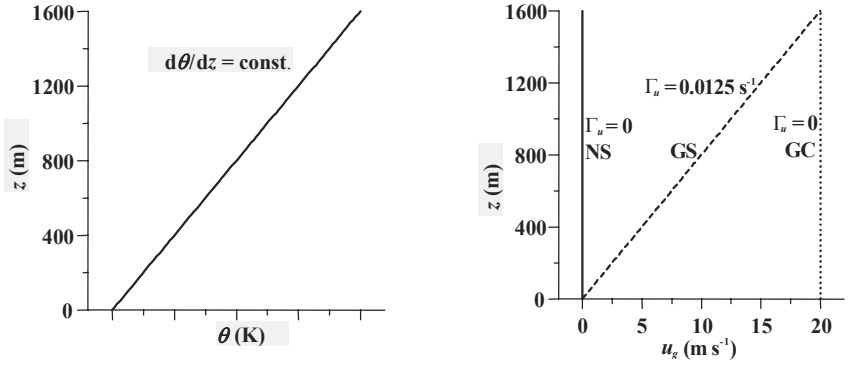


Fig. 2. Initial profiles of the potential temperature $\theta$ (left plot) and the $x$-component of the geostrophic wind velocity $u_g$ (right plot) for CBL cases simulated in Conzemius and Fedorovich (2006a). In the right plot, the solid line represents the NS-case simulation, the dotted line the GC-case simulation (Section 3.1), and the dashed line the GS-case simulation (Section 3.2).

Three gradations of outer (free-atmosphere) flow stratification were studied: $\partial\theta/\partial z = 0.001$, 0.003, and 0.010 K m$^{-1}$ (in terms of the Brunt–Väisälä frequency: $N = 0.006$, 0.010, and 0.018 s$^{-1}$). The adopted values of surface kinematic heat flux $Q_s$ were 0.03, 0.1, and 0.3 K m s$^{-1}$. The chosen value of 20 m s$^{-1}$ for initial momentum in the flow provided a strong surface shear that is, albeit strong, is not unrealistic for atmospheric CBLs.

The effects of shear on the CBL growth rate in the conducted simulations turned out to be heavily dependent on the combination of stratification and surface buoyancy flux. In general, the effects of shear stood out the most when the surface buoyancy flux was weakest, but they also appeared to be stronger when the free atmospheric stratification was weak. A strong enhancement of CBL growth in the GC *versus* the NS case is seen in Figs. 3d and 3g, and a weaker enhancement is observed in Figs. 3b and 3e. On the other hand, Figs. 3c, 3f, and 3h show no enhancement, and Fig. 3i even points to the decreased growth rate of sheared CBL compared to the shear-free CBL.

Conzemius and Fedorovich (2006a) came to the following two general conclusions regarding the enhancement of CBL growth by shear in the barotropic case. First, the elevated shear, which fast develops with time at the CBL top, is a primary factor of the CBL growth acceleration in this case. Second, this elevated shear build-up is characteristic of relatively slowly growing CBL cases with either weaker heat flux or stronger outer stratification, when the surface friction has the longest time to reduce the momentum in the mixed layer.

The cases with $\partial\theta/\partial z = 0.003$ K m$^{-1}$ and $Q_s = 0.003$ K m s$^{-1}$ were chosen in *op. cit.* for a more detailed analysis of the shear influence on the barotropic CBL structure and evolution. At earlier stages in the simulations, the TKE production terms and velocity profiles in Fig. 4 indeed show the elevated shear to be making the bulk of the contribution to the enhanced entrainment in the GC case. In the velocity profiles, the value of $u$ in the interior of the CBL decreases very quickly early in the simulation and

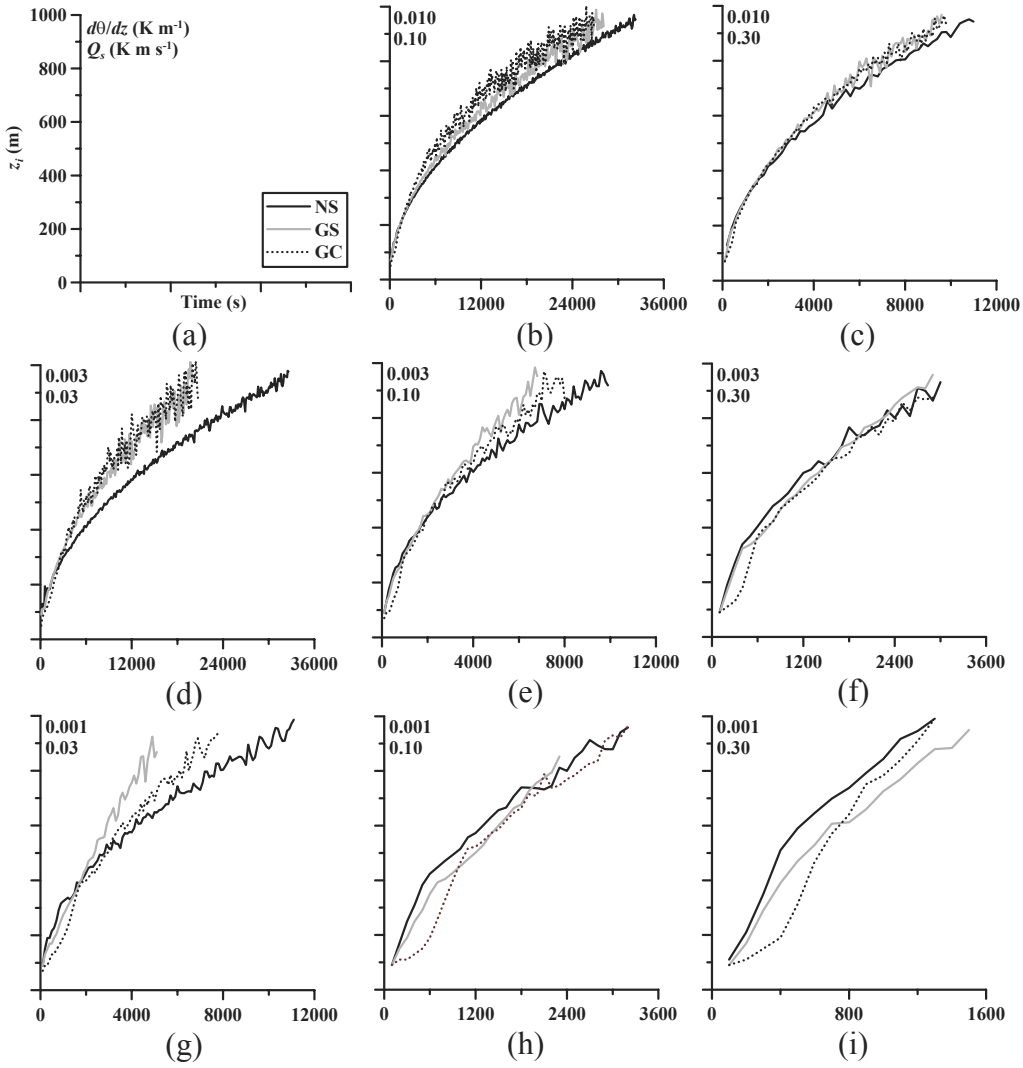


Fig. 3. Depth of the CBL, $z_i$ (m), as a function of time (s) for the CBL cases with different $\partial\theta/\partial z$ and $Q_s$ (the values are indicated in the upper left corners of the plots) numerically studied in Conzemius and Fedorovich (2006a).

the entrainment zone shear is rather large already at this stage of the CBL development. The overall increment of $u$ across the entrainment zone then changes very little between $t = 2500$ s and $t = 20{,}000$ s, maintaining a value of about 4 m s$^{-1}$. Meanwhile, the $v$ profiles show a substantial increase in the $v$ increment across the entrainment zone, from roughly 4 m s$^{-1}$ at $t = 2500$ s to about 6 m s$^{-1}$ at $t = 20{,}000$ s. Since the shear production of TKE is roughly proportional to the product of the square of velocity increment and the CBL growth rate d$z_i$/d$t$, the shear contribution to the integral TKE budget is cut in half over the considered period of time.

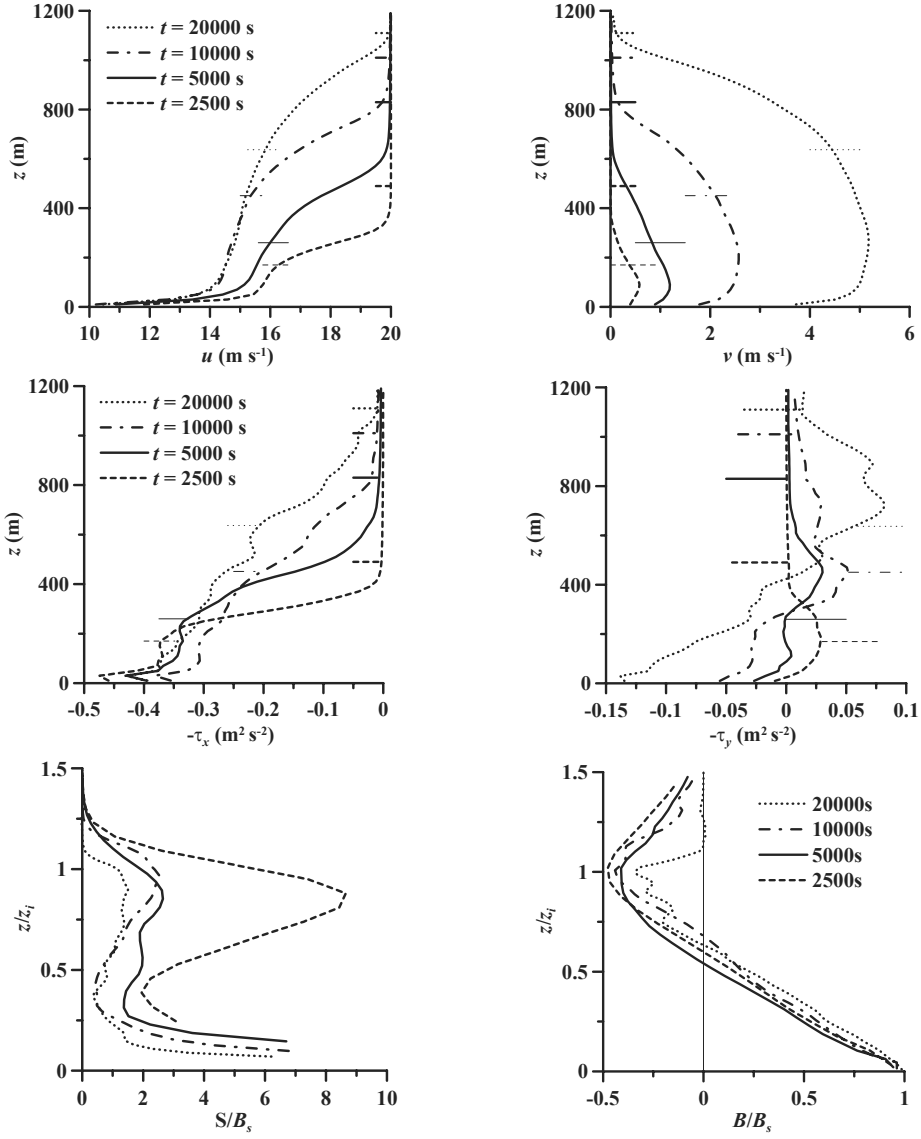


Fig. 4. Evolution of the $x$ and $y$ mean wind components ($u$ and $v$; two upper plots), vertical momentum flux components ($-\tau_x$ and $-\tau_y$; two middle plots), and normalized TKE budget shear $S$ and buoyancy $B$ production terms for the GC-case CBL with $\partial\theta/\partial z = 0.003$ K m$^{-1}$ and $Q_s = 0.03$ K m s$^{-1}$ (two bottom plots). Profiles correspond to four times in the simulation. From Conzemius and Fedorovich (2006a).

From the evolution of the vertical momentum flux profiles in Fig. 4, one can see that the $x$ component of momentum flux is a fair bit larger than the $y$ component. Both flux components exhibit a substantial change across the entrainment zone, approach-

ing zero near the top of the entrainment zone, as turbulence diminishes. In general, the magnitude of the momentum flux in the entrainment zone shows a gradual decrease with time, and this decrease is directly related to the decreasing CBL growth rate $dz_i/dt$ during the simulations. The decreasing momentum entrainment leads to a weaker shear production of turbulence as further shown in Fig. 4.

The profiles of shear production term in the TKE budget are plotted with the $z_i$-normalized vertical coordinate in order to show the location of the production relative to $z_i$. The surface shear generation of TKE, which does not change considerably during the simulation, is truncated in the plot in order to highlight the TKE production by entrainment-zone shear. The buoyancy production of TKE in the lower CBL portion does not considerably change in the course of simulation, but the consumption of TKE in the entrainment zone noticeably decreases with time. At no stage of the simulation did any of the TKE transport profiles (not shown) indicate enhanced transport from the surface into the entrainment zone. Those observations allowed to conclude that the enhancement of the entrainment flux ratio in the barotropic sheared CBL is most directly tied to the entrainment-zone shear production of turbulence – not to the upward transport of surface shear-generated TKE.

It was additionally found that fraction of the shear-produced TKE spent on entrainment is no higher than 0.5 once the entrainment reaches a relatively steady state. This suggests that fractions of 0.7 or higher, suggested in Price *et al*. (1978), and used in model studies of Tennekes and Driedonks (1981), Driedonks (1982), Boers (1984), and Pino *et al*. (2003), are probably overestimates.

Numerical investigation by Conzemius and Fedorovich (2006a) of the behavior of the gradient and flux Richardson numbers in the entrainment zone of the barotropic CBL revealed sublayers of nearly constant Ri over much of the entrainment zone in those CBL cases where the shear contribution to the TKE budget at the entrainment zone was relatively large, see also gradient Ri profiles in Kim *et al*. (2003) and Ri-number considerations in Sorbjan (2004). The GC-case simulation featured a layer of constant Ri inside the entrainment zone, with both gradient and flux Ri number having values about 0.25 and staying approximately constant in the face of changing shear and temperature stratification. The constancy of Ri within the entrainment zone manifested a local balance between the turbulence generation by shear and the turbulence destruction associated with negative buoyancy flux, dissipation, or energy drain out of the entrainment zone.

Fedorovich *et al*. (2004a) brought together six representative LES codes with an aim to investigate main characteristics of turbulence structure and growth dynamics of sheared CBLs as reproduced by LES of different architecture, with different numerical algorithms, different spatial and temporal resolution, and featuring different subgrid-turbulence and surface-layer parameterizations. The participating LES codes represented University of Oklahoma (OU; Fedorovich *et al*. 2001a, 2004b), National Center for Atmospheric Research (NCAR; Moeng 1984 and Sullivan *et al*. 1998), West Virginia University (WVU; Sykes and Henn 1989; Lewellen and Lewellen 1998), Nansen Environmental and Remote Sensing Center, Norway (NERSC; Esau 2004), Center for

Analysis and Prediction of Storms, OU (ARPS; Xue *et al*. 2000, 2001), and Institute for Space Studies of Catalonia, Spain / Wageningen University, the Netherlands (BUW; Cuijpers and Duynkerke 1993, Cuijpers and Holtslag 1998, and Pino *et al*. 2003). All codes were run in a simulation domain of $X \times Y \times Z = 10 \times 10 \times 2$ km$^3$ (slight deviations from these basic dimensions were allowed) with periodic lateral boundary conditions. Three atmospheric CBL cases were reproduced – all with the same surface virtual potential temperature flux (0.1 K m s$^{-1}$) and the same thermal stratification in the free atmosphere above the CBL (0.003 K m$^{-1}$), but with three different shear forcings.

For the case of the barotropic CBL, the prescribed shear forcing was the same as in Conzemius and Fedorovich (2006a), see the GC case data in Fig. 2. All participated codes predicted evolution of the mean CBL temperature field in a rather close manner. The codes also fairly agreed in prediction of the increase of the entrainment-zone depth and the magnitude of the entrainment heat flux in the sheared CBL. As can be expected, the horizontal velocity variance was found to be significantly larger throughout the depth of the CBL in the presence of the mean wind shear. The vertical velocity ($w$) component variance was found to be larger throughout most of the CBL compared to its values in the shear-free CBL. Additionally, vertical velocity variance retained much higher values throughout the entrainment zone in the sheared CBL than in the shear-free entrainment layer, so that the rapid decay of variance towards the CBL top, characteristic of the shear-free case, was replaced in the sheared CBL by a secondary maximum. However, the enhancement of vertical velocity fluctuations in the interior of the sheared CBL appeared to be heavily code-dependent, so it was difficult to make any definitive conclusion regarding the modification of the turbulence regime there.

The third-order moments of vertical velocity and virtual potential temperature fluctuations also exhibited a considerable code-to-code variability. Despite that, all codes captured certain features of the higher-order CBL turbulence structure under the influence of shear in a common manner. For example, all the codes agreed on the change of sign of $\overline{\theta'\theta'\theta'}$ in the middle of the entrainment zone, pointing to the positively skewed temperature fluctuations in the lower portion of the entrainment zone, just beneath the capping inversion, and strongly negatively skewed fluctuations in the upper portion of the entrainment zone, where the magnitude of $\overline{\theta'\theta'\theta'}$ was several times larger than in the layer just below the inversion. The amplitude of the $\overline{\theta'\theta'\theta'}$ variations across the entrainment layer was larger in the sheared CBL (GC) case, while in the absence of mean wind shear, these variations were comparatively small. Over the main portion of the sheared CBL, the positive $\overline{w'w'w'}$ was an active contributor to the transport of the surface shear-generated turbulence upward, into the bulk of the layer. Throughout the entrainment layer of the sheared CBL, all codes predicted essentially negative values of $\overline{w'w'w'}$. This could possibly be an indication of narrow sweeping downward motions associated with the breaking of Kelvin-Helmholtz billows at the sheared density interface (temperature inversion). Contribu-

tion of these motions to the entrainment could be a reason for larger entrainment heat flux values observed in the sheared CBL cases.

All codes consistently predicted deeper CBLs when the CBL depth $z_i$ was determined from the elevation of the strongest temperature gradient (maximum inversion) than when $z_i$ was estimated from the height of the kinematic heat flux minimum within the entrainment layer. The fact that the temperature-gradient method yields larger CBL depth values than the heat flux minimum approach, at least for the shear-free CBL, is rather well known. It has been discussed, *e.g.*, in Sullivan *et al*. (1998) and Fedorovich *et al*. (2004b). On the other hand, the temperature-gradient method provided a smoother dependence of $z_i$ on $t$ as compared to $z_i$ determined from the statistically less steady heat-flux data. In the presence of shear, the CBL grew considerably faster than its shear-free counterpart with the same buoyancy forcings, and differences between the CBL depths, determined by the temperature-gradient and heat-flux methods, were generally larger.

### 3.2 Equivalent barotropic CBL

Compared to the effects of surface shear, the influence of elevated wind shears on the CBL dynamics is much less studied numerically and experimentally. Such shears are typically observed in the atmospheric CBL under baroclinic and equivalent barotropic conditions (Stull 1988) with magnitudes of wind velocity increments across the CBL being dependent on the rate of geostrophic wind change with height.

Brown (1996) performed LES of the equivalent barotropic sheared CBL and compared the resulting velocity variance profiles with predictions from one-dimensional CBL models. In this study, which was primarily focused on the behavior of turbulence statistics in the CBL interior, the effects of entrainment were eliminated by imposing rigid-lid boundary conditions at the top of the domain. The author acknowledged that entrainment effects would need to be considered before the results could be generalized for the atmospheric CBL, and that coupling between shear across the CBL top and the entrainment could modify the CBL dynamics.

The simulated CBL case with the height-dependent geostrophic wind in the study of Pino *et al*. (2003), (see Section 3.1), had the largest CBL growth rate and showed the best agreement, among the three investigated cases, with the observed atmospheric CBL growth rate. According to data from their simulation with geostrophic shear (denoted as BGS in Fig. 1), the shear at the inversion level leads to the decrease of the buoyancy term in the TKE budget (which is equivalent to the increase of its absolute value) at this level compared to the CBL with the surface shear only. The dissipation term also increases in order to compensate the increased shear term, which was the largest in the case with geostrophic shear (among three CBL cases considered in *op. cit*). Pressure and transport terms in this regime appear to be rather small in magnitude and mutually compensating (see Fig. 1c). One may notice also that with increasing contribution of the elevated shear to the TKE production at the CBL top, the heat/buoyancy entrainment region identified by negative values of the buoyancy flux is expanding vertically. Based on these LES results, Pino *et al*. (2003) concluded that

it is advisable to include the contribution of shear in a parameterization of the entrainment flux.

Conzemius and Fedorovich (2006a) arrived at a similar conclusion. They found, however, that it is the **elevated shear** that has to be parameterized in models of entrainment in order to improve their performance. The CBLs in the GC cases from Conzemius and Fedorovich (2006a) consistently had strong surface layer shear but never exhibited more rapid growth than in the GS cases (schematically shown in Fig. 2), except when the entrainment zone shear was stronger. This suggests that surface shear does not play a direct role in increasing the CBL growth rate, but indirectly, the slower CBL flow, in general, causes shear to develop at the CBL top.

The increment of $u$, across the entrainment zone in the GS-case CBL, increases dramatically during the simulation (see Fig. 5). Shear in the $v$ profile also increases with time. The corresponding momentum-flux profiles in Fig. 5 show that the $x$-component flux is the dominant one, and its magnitude increases throughout the simulation as the growing CBL encounters ever-greater momentum at its top. Accordingly, the shear generation of TKE increases during the simulation as long as the shear magnitude at the CBL top increases. This increase in TKE production by shear is accompanied by the increase of the buoyancy consumption of TKE (see two bottom plots in Fig. 5) – the effect that was earlier pointed out by Pino *et al*. (2003).

The above considerations indicate that the entrainment flux ratio in the GS-case CBL, like in the previously analyzed GC-case CBL (Section 3.1), appears to be directly related to the shear across the entrainment zone. In the equivalently barotropic CBL (GS case), the entrainment-zone shear is initially zero and increases during the simulation. This increase, accompanied by increasing momentum flux, results in the intensive generation of TKE at the inversion level and increase in the entrainment-flux ratio. In the GC-case CBL (barotropic CBL), on the other hand, the entrainment-zone shear is significant only when the CBL first becomes established. Thereafter, due to the slowing CBL growth, the entrainment-zone shear production of turbulence decreases, which results in a smaller entrainment flux ratio with time.

The analysis by Conzemius and Fedorovich (2006a) clearly showed that it is the shear production of TKE resulting from entrainment zone shear, *not* the upward transport of surface shear-generated TKE, which drives the enhanced entrainment in sheared CBLs. As one may conclude from comparison of the CBL depth evolution plots (see Fig. 3), in the equivalent barotropic GS-case CBLs, which feature the background shear, larger shear accumulation takes place at the CBL top, and the GS CBL growth is generally faster than the GC CBL growth. This relationship between the entrainment rates of GS and GC cases is not always the same, however. In Fig. 3b, for instance, the growth of the GC-case CBL outpaces that of the GS-case CBL, highlighting the following Conzemius and Fedorovich (2006a) findings regarding the role of shear across the entrainment zone: (*i*) the entrainment zone shear plays a more direct role in enhancing CBL growth as compared to the surface shear, and (*ii*) that the effects of surface shear on the CBL growth are only felt indirectly through the reduction of the mixed layer velocity and resulting increase of shear at the CBL top.

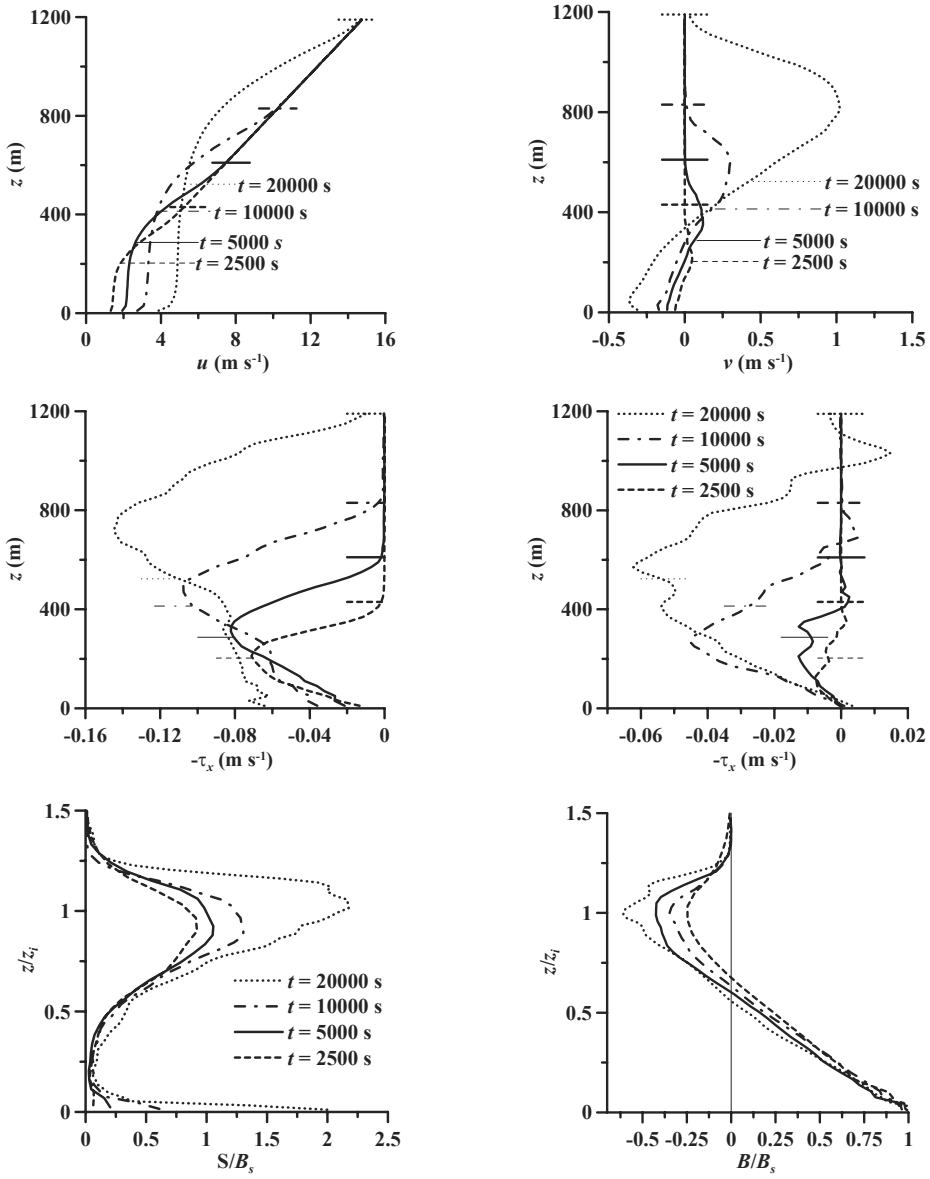


Fig. 5. Evolution of the $x$ and $y$ mean wind velocity components ($u$ and $v$; two upper plots), vertical momentum flux components ($-\tau_x$ and $-\tau_y$; two middle plots), and normalized TKE budget shear $S$ and buoyancy $B$ production terms for the GS-case CBL with $\partial\theta/\partial z$ = 0.003 K m$^{-1}$ and $Q_s$ = 0.03 K m s$^{-1}$ (two bottom plots). Profiles correspond to four times in the simulation. From Conzemius and Fedorovich (2006a).

Additionally, Conzemius and Fedorovich (2006a) found that, for CBL cases in which the shear contribution to the entrainment zone TKE budget was relatively large, the gradient and flux Richardson numbers are nearly constant over most of the en-

trainment zone in the equivalent barotropic CBL (GS case), much as they are in the GC-case CBL (Section 3.1).

In the sheared CBL LES comparison study of Fedorovich *et al*. (2004a), all participating codes generally agreed on the enhanced growth rate of the equivalent barotropic CBL (GS case) as compared to the purely barotropic CBL (GC case). That study also revealed some distinctive features of the CBL structure in the GS case. While shear and shear production of TKE in the GS-case CBL were concentrated predominantly at the CBL top, the vertical transport of TKE (represented by $\overline{w'w'w'}$) appeared to be close to zero in this region, so that the shear-generated turbulence remained locked in the upper portion of the CBL.

### 3.3 Baroclinic CBL

Sorbjan (2004) accounted for effects of baroclinicity and temperature advection in the LES of sheared CBL by including in the governing LES equations additional terms associated with horizontal gradients of the reference (background) potential temperature field. This allowed periodic boundary conditions for the deviation of the potential temperature from its reference value to be kept. By means of such modified LES, Sorbjan (2004) investigated four CBL flow cases characterized by different contributions of shear and temperature advection to the CBL dynamics and evaluated results against a barotropic CBL case with a height-constant geostrophic wind. Depending on the prescribed values of the angle between the horizontal gradients of pressure and potential temperature and vertical gradients of the geostrophic wind components, these four studied cases were denoted, respectively, as positive-shear case, warm-advection case, negative-shear case, and cold-advection case.

The main object of the study was the CBL turbulence structure and, particularly, the fine features of this structure within the inversion layer (entrainment zone). The outer (free-atmosphere) stratification was set to be very strong and the surface buoyancy flux was taken constant, so CBL growth rates did not differ drastically among the cases. Moreover, the data used for comparison of different CBL cases were collected at the CBL evolution stages characterized by very close values of integral parameters of the layer, such as friction velocity $u_*$, convective velocity $w_*$, inversion height $z_i$, and $-L/z_i$ ratio.

Mean flow parameters and turbulence statistics from the conducted runs were presented in the normalized form using the Deardorff (1970b) convective scales: $z_i$ for height, $w_* = (\beta Q_s z_i)^{1/3}$ for velocity, and $\theta_* = Q_s / w_*$ for potential temperature, where $Q_S$ is the surface kinematic heat flux (and $\beta Q_S$ is the surface buoyancy flux).

With the chosen thermal advection forcing, the strongest effects of different shear configurations were found in the mean profiles of velocity components and potential temperature. The manner of profile changes caused by geostrophic shear was, however, different for velocity component and temperature profiles. The velocity profiles were affected with respect to both magnitude and shape (Fig. 6), while the temperature

profile shapes exhibited only slight modification over the main portion of the CBL, and the principal effect of temperature advection was in shifting profiles laterally with respect to each other (Fig. 7).

One may observe a remarkable correlation between profiles of momentum flux components (lower plots in Fig. 6) and vertical gradients of the corresponding mean velocity components (upper plots of Fig. 6). Turbulent warming rates associated with convective heating from the ground were close to each other for all considered cases,

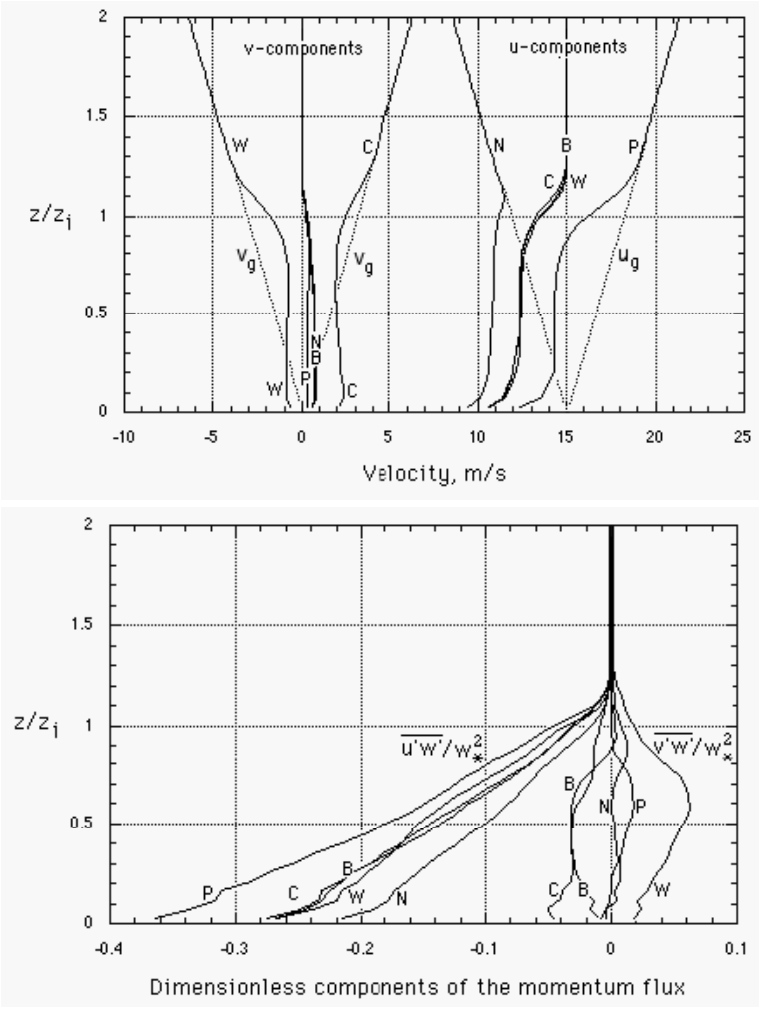


Fig. 6. Profiles of the mean wind components (upper plot; *u* is on the right, *v* is on the left; components of the geostrophic wind are indicated by dotted lines) and components of the kinematic turbulent momentum flux (lower plot) from five LES runs of Sorbjan (2004, with kind permission of Springer Science and Business Media): B – barotropic, W – with warm advection, C – with cold advection, P – with positive shear, and N – with negative shear.

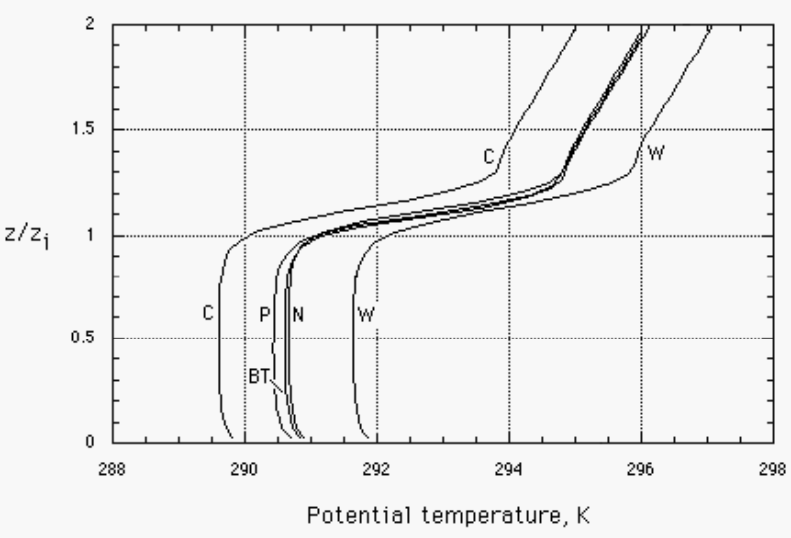


Fig. 7. Profiles of the mean potential temperature (upper plot) and turbulent kinematic heat (temperature) flux (lower plot) from five LES runs of Sorbjan (2004, with kind permission of Springer Science and Business Media). Explanations as in Fig. 6.

so kinematic heat flux profiles for different cases did not differ much over the main portion of the CBL. The effects of thermal advection were more noticeable in the entrainment-zone region, shown in Fig. 9 of Sorbjan (2004), as the interval of heights with negative heat flux values.

The profiles of turbulence variances of vertical velocity and potential temperature from the Sorbjan (2004) study display similar tendencies: the variances for different CBL cases do not deviate considerably from each other within the main portion of the CBL, but in the entrainment zone, they start to show consistent dependence on the shear/thermal advection forcing.

Such tendencies are clearly seen in the profiles of vertical velocity and potential temperature variances shown in Fig. 8. Remarkably, almost all vertical velocity variance profiles in this plot show secondary maxima throughout the interfacial layer that have also been predicted by different LES codes in the comparison study described in Section 3.1.

In the profiles of horizontal velocity variance (not shown) from Sorbjan (2004), these interfacial-layer effects were somewhat obscured because of the strong influence of the simulated shear forcings on the horizontal velocity fields. These behavioral features of turbulence statistics led Sorbjan (2004) to a conclusion that flow in the baroclinic CBL under the effect of shear is split vertically in two regions. In the lower one – that is within the core part of the layer – the flow is controlled by heating from the surface. The Deardorff (1970b) convective scales are appropriate for description of this part of the CBL flow. On the other hand, in the upper region – that is within the

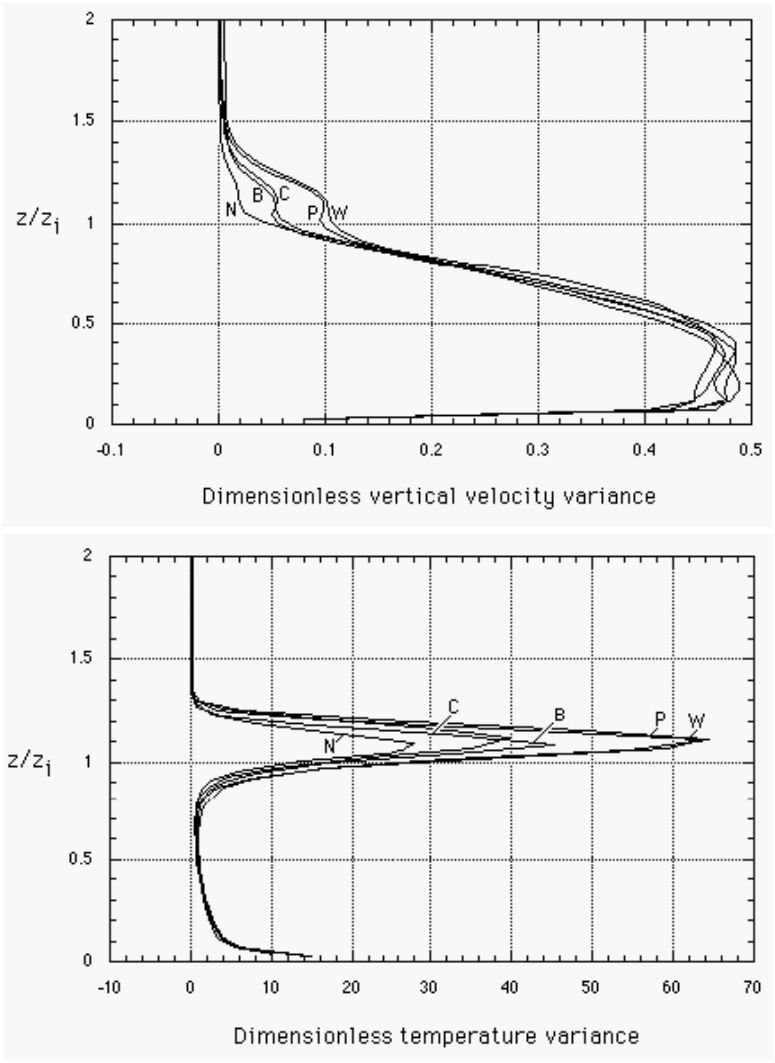


Fig. 8. Profiles of the vertical velocity variance scaled with $w_*^2$ (upper plot) and potential temperature variance scaled with $\theta_*^2$ (lower plot) from five LES runs of Sorbjan (2004, with kind permission of Springer Science and Business Media). Explanations as in Fig. 6.

interfacial (entrainment) layer – the flow is controlled by stratification and shear. For the flow in this region, Sorbjan (2004) proposed a special Richardson-number based scaling, which has been evaluated for the entraining sheared CBL by Conzemius and Fedorovich (2006b, 2007) and found to agree relatively well with LES data. Apparently, the two-layer concept for barotropic and equivalent barotropic sheared CBLs was first suggested by Lewellen and Lewellen (2000), who indicated that a sheared CBL can be considered as two separate turbulent layers: a buoyancy-driven mixed layer topped by a shear-driven layer.

## 4. SUMMARY

Below, we summarize main elements of modern conceptual understanding of the role that wind shears play in modification of the CBL structure and evolution.

- First, the presence of wind shears may essentially modify the structure of mean flow and turbulence in the CBL. As the contribution of wind shear to the turbulence production increases, the coherent turbulence structure in the CBL changes from quasi-hexagonal cells to horizontal convective rolls, which are oriented parallel to the mean flow vector. Also, increased shear is associated with larger velocity component and potential temperature variances and with enhanced vertical momentum transport throughout the CBL. The vertical distribution of second- and third-order order turbulence statistics of the flow parameters in the upper portion of sheared CBL often show peculiar features that are presumably associated with interaction between the buoyancy (stratification) and shear forcings in the capping inversion layer. In the bulk of the layer, third-order moments of vertical velocity and potential temperature are affected by shear much less, in a relative sense, than their second-order counterparts (variances), which leads to reduced skewness of vertical velocity and potential temperature in sheared CBLs compared to shear-free CBLs.

- Second, it is wind shear across the entrainment zone (elevated shear) that directly contributes to the intensification of the entrainment and CBL growth rate. The surface layer shear plays little, if any, direct role in the enhancement of entrainment in sheared CBLs. This conclusion supports findings from previous studies, which have suggested that most of the surface shear-generated TKE dissipates locally. On the other hand, the surface shear has an indirect effect on entrainment by slowing the flow in the CBL interior and causing the development of shear at the top of the CBL, and it is this entrainment zone shear that enhances the entrainment.

- Third, the atmospheric CBL may be considered as a single-layer entity in the shear-free case. When wind shear is present, the CBL acquires a two-layer structure, composed of a layer of height-constant buoyancy and velocity, which is similar to the shear-free CBL, topped by a shear-driven layer whose turbulence is maintained by a balance among shear generation of TKE, buoyancy consumption of TKE, and dissipation.

- Fourth, when shear makes a substantial contribution to the TKE generation in the entrainment zone, sheared CBLs exhibit a layer of nearly constant gradient Richardson number, as well as flux Richardson number, within the entrainment zone (interfacial layer). The gradient Richardson number of about 0.25 can be taken as a characteristic value under conditions when the shear production of TKE in the entrainment zone is significant compared to the buoyancy production of turbulence. The value of flux Richardson number is typically within the range from 0.2 to 0.4 whenever shear enhancement of CBL growth is observed. The local constancy of flux Richardson number within the entrainment manifests a balance between the turbulence generation by shear and the turbulence destruction associated with negative buoyancy flux, dissipation, or energy drain out of the entrainment zone. When the shear contri-

bution to the TKE production is less dominant, the Richardson number in the entrainment zone becomes variable. It grows as the shear decreases, increasing to infinity when the shear approaches zero.

- Fifth, the fraction of the shear-produced TKE used for entrainment in sheared CBLs is no higher than 0.5 once the entrainment reaches a relatively steady state. This indicates that previously suggested fractions of 0.7 or higher are probably overestimates.

Acknowledgement. The presented research has been supported, in part, by the National Science Foundation, USA, through the grant ATM-0124068.

## References

Angevine, W.M. (1999), Entrainment results including advection and case studies from the Flatland boundary layer experiments, *J. Geophys. Res*. **104**, 30,947-30,963.

Angevine, W.M., H.K. Baltink, and F.C. Bosveld (2001), Observations of the morning transition of the convective boundary layer, *Bound.-Layer Meteor*. **101,** 209-227.

Arya, S.P.S., and J.C. Wyngaard (1975), Effect of baroclinicity on wind profiles and the geostrophic drag law for the convective planetary boundary layer, *J. Atmos. Sci*. **32**, 767-778.

Barr, A.G., and G.S. Strong (1996), Estimating regional surface heat and moisture fluxes above prairie cropland from surface and upper air measurements, *J. Atmos. Sci*. **35**, 1716-1735.

Batchvarova, E., and S.-E. Gryning (1991), Applied model for the growth of the daytime mixed layer, *Bound.-Layer Meteor*. **56**, 261-274.

Batchvarova, E., and S.-E. Gryning (1994), An applied model for the height of the daytime mixed layer and the entrainment zone, *Bound.-Layer Meteor*. **71**, 311-323.

Betts, A.K. (1974), Reply to comment on the paper "Non-precipitating Cumulus Convection and its Parameterization", *Quart. J. Roy. Meteorol. Soc*. **100**, 469-471.

Betts, A.K., and J.H. Ball (1994), Budget analysis of FIFE 1987 sonde data, *J. Geophys. Res*. **99**, 3655-3666.

Betts, A.K., and A.G. Barr (1996), First International Satellite Land Surface Climatology Field Experiment 1987 sonde budget revisited, *J. Geophys. Res*. **101**, 23285-23288.

Betts, A.K., R.L. Desjardins, and J.I. MacPherson (1992), Budget analysis of the boundary layer grid flights during FIFE 1987, *J. Geophys. Res*. **97**, 18533-18546.

Boers, R., E.W. Eloranta, and R.L. Coulter (1984), Lidar observations of mixed layer dynamics: tests of parameterized entrainment models of mixed layer growth rate, *J. Climate Appl. Meteor.* **23**, 247-266.

Brost, R.A., D.H. Lenschow, and J.C. Wyngaard (1982a), Marine stratocumulus layers. Part I: Mean conditions, *J. Atmos. Sci*. **39**, 800-817.

Brost, R.A., D.H. Lenschow, and J.C. Wyngaard (1982b), Marine stratocumulus layers. Part II: Turbulence budgets, *J. Atmos. Sci*. **39**, 818-836.

Brown, A.R. (1996), Large-eddy simulation and parameterisation of the baroclinic boundary-layer, *Quart. J. Roy. Meteor. Soc*. **122,** 1779-1798.

Caughey, and S.G. Palmer (1979), Some aspects of turbulence structure through the depth of the convective boundary layer, *Quart. J. Roy. Meteor. Soc*. **105**, 811-827.

Chou, S.-H., D. Atlas, and E.-N. Yeh (1986), Turbulence in a convective marine atmospheric boundary layer, *J. Atmos. Sci*. **43**, 547-564.

Conzemius, R.J., and E. Fedorovich (2006a), Dynamics of sheared convective boundary layer entrainment. Part I: Methodological background and large eddy simulations, *J. Atmos. Sci.* **63**, 1151-1178.

Conzemius, R.J., and E. Fedorovich (2006b), Dynamics of sheared convective boundary layer entrainment. Part II: Evaluation of bulk model predictions of entrainment flux, *J. Atmos. Sci*. **63**, 1179-1199.

Conzemius, R., and E. Fedorovich (2007), Bulk models of the sheared convective boundary layer: evaluation through large eddy simulations, *J. Atmos. Sci*. **64**, 786-807.

Cuijpers, J.W.M., and P.G. Duynkerke (1993), Large eddy simulation of trade wind cumulus clouds, *J. Atmos. Sci*. **50**, 3894-3908.

Cuijpers, J.W.M., and A.A.M. Holtslag (1998), Impact of skewness and nonlocal effects on scalar and buoyancy fluxes in convective boundary layers, *J. Atmos. Sci*. **55**, 151-162.

Davis, K.J., D.H. Lenschow, S.P. Oncley, C. Kiemle, G. Ehret, A. Giez, and J. Mann (1997), Role of entrainment in surface-atmosphere interactions over the boreal forest*, J. Geophys. Res.* **102**, 29219-29230.

Deardorff, J.W. (1970a), Preliminary results from numerical integration of the unstable boundary layer, *J. Atmos. Sci*. **27**, 1209-1211.

Deardorff, J.W. (1970b), Convective velocity and temperature scales for the unstable planetary boundary layer and for Raleigh convection, *J. Atmos. Sci*. **27**, 1211-1213.

Deardorff, J.W. (1972), Numerical investigation of neutral and unstable planetary boundary layers, *J. Atmos. Sci*. **29**, 91-115.

Deardorff, J.W. (1979), Prediction of convective mixed-layer entrainment for realistic capping inversion structure, *J. Atmos. Sci*. **36**, 424-436.

Deardorff, J.W., G.E. Willis, and D.K. Lilly (1969), Laboratory investigation of nonsteady penetrative convection, *J. Fluid Mech*. **35**, 7-31.

Driedonks, A.G.M. (1982), Models and observations of the growth of the atmospheric boundary layer, *Bound.-Layer Meteor.* **23**, 283-306.

Esau, I. (2004), Simulation of Ekman boundary layers by large eddy model with dynamic mixed subfilter closure, *J. Env. Fluid Mech*. **4**, 273-303.

Fedorovich, E. (1995), Modeling the atmospheric convective boundary layer within a zero-order jump approach: an extended theoretical framework, *J. Appl. Meteor*. **34**, 1916-1928.

Fedorovich, E. (1998), Bulk models of the atmospheric convective boundary layer. **In:** E.J. Plate *et al*. (eds.), *Buoyant Convection in Geophysical Flows*, Kluwer Academic Publishers, Dordrecht, 265-290.

Fedorovich, E., and R. Kaiser (1998), Wind tunnel model study of turbulence regime in the atmospheric convective boundary layer. **In:** E.J. Plate *et al*. (eds.), *Buoyant Convection in Geophysical Flows*, Kluwer Academic Publishers, Dordrecht, 327-370.

Fedorovich, E., and D.V. Mironov (1995), A model for a shear-free convective boundary layer with parameterized capping inversion structure, *J. Atmos. Sci*. **52,** 83-95.

Fedorovich, E., and J. Thäter (2001), Vertical transport of heat and momentum across a sheared density interface at the top of a horizontally evolving convective boundary layer, *J. Turbulence* **2**, 7, 1-17, DOI: 10.1088/1468-5248/2/1/007.

Fedorovich, E., R. Kaiser, M. Rau, and E. Plate (1996), Wind tunnel study of turbulent flow structure in the convective boundary layer capped by a temperature inversion, *J. Atmos. Sci*. **53**, 1273-1289.

Fedorovich, E., F.T M. Nieuwstadt, and R. Kaiser (2001a), Numerical and laboratory study of horizontally evolving convective boundary layer. Part I: transition regimes and development of the mixed layer, *J. Atmos. Sci*. **58,** 70-86.

Fedorovich, E., F.T.M. Nieuwstadt, and R. Kaiser (2001b), Numerical and laboratory study of horizontally evolving convective boundary layer. Part II: effects of elevated wind shear and surface roughness, *J. Atmos. Sci*. **58,** 546-560.

Fedorovich, E., R. Conzemius, I. Esau, F. Katapodes-Chow, D. Lewellen, C.-H. Moeng, P. Sullivan, D. Pino, and J.V.-G. de Arellano (2004a), Entrainment into sheared convective boundary layers as predicted by different large eddy simulation codes. **In:** *Preprints, 16th Symp. on Boundary Layers and Turbulence, 9-13 August, Amer. Meteor. Soc. Portland, ME*, CD-ROM, P4.7.

Fedorovich, E., R. Conzemius, and D. Mironov (2004b), Convective entrainment into a shear-free linearly stratified atmosphere: bulk models re-evaluated through large eddy simulations, *J. Atmos. Sci*. **61**, 281-295.

Flamant, C., J. Pelon, P.H. Flamant, and P. Durand (1997), Lidar determination of the entrainment zone thickness at the top of the unstable marine atmospheric boundary layer, *Bound.-Layer Meteor*. **83,** 247-284.

Garratt, J.R., and J.C. Wyngaard (1982), Winds in the atmospheric convective boundary layer – prediction and observation, *J. Atmos. Sci*. **39**, 1307-1316.

Grossman, R.L. (1992), Convective boundary layer budgets of moisture and sensible heat over an unstressed prairie, *J. Geophys. Res*. **97,** 18425-18438.

Holtslag A.A.M, and P.G. Duynkerke, eds., (1998), *Clear and Cloudy Boundary Layers*, Royal Netherlands Academy of Arts and Sciences, Amsterdam, 372 pp.

Holtslag, A.A.M., and F.T.M. Nieuwstadt (1986), Scaling the atmospheric boundary layer, *Bound.-Layer Meteor*. **36**, 201-209.

Hoxit, L.R. (1974), Planetary boundary layer winds in baroclinic conditions, *J. Atmos. Sci*. **31**, 1003-1020.

Kaimal, J.C., J.C. Wyngaard, D.A. Haugen, O.R. Coté, Y. Izumi, S.J. Caughey, and C.J. Readings (1976), Turbulence structure in a convective boundary layer, *J. Atmos. Sci*. **33**, 2152-2169.

Kaiser, R., and E. Fedorovich (1998), Turbulence spectra and dissipation rates in a wind tunnel model of the atmospheric convective boundary layer, *J. Atmos. Sci*. **55**, 580-594.

Khanna, S., and J.G. Brasseur (1998), Three-dimensional buoyancy and shear-induced local structure of the atmospheric boundary layer, *J. Atmos. Sci*. **55**, 710-743.

Kim, S.-W., and S.-U. Park (2003), Coherent structures near the surface in a strongly sheared convective boundary layer generalized by large-eddy simulation, *Bound.-Layer Meteor*. **106**, 35-60.

Kim, S.-W., S.-U. Park, and C.-H. Moeng (2003), Entrainment processes in the convective boundary layer with varying wind shear, *Bound.-Layer Meteor*. **108**, 221-245.

Kim, S.-W., S.-U. Park, D. Pino, and J.V.-G. de Arellano (2006), Entrainment parameterization in a sheared convective boundary layer by using a first-order jump model, *Bound.-Layer Meteor.* **120**, 455-475.

Lemone, M.A. (1973), The structure and dynamics of horizontal roll vortices in the planetary boundary layer, J. *Atmos. Sci*. **30**, 1077-1091.

Lemone, M.A., M. Zhou, C.-H. Moeng, D.H. Lenschow, L.J. Miller, and R.L. Grossman (1999), An observational study of wind profiles in the baroclinic convective mixed layer, *Bound.-Layer Meteor*. **90**, 47-82.

Lenschow, D.H. (1970), Airplane measurements of planetary boundary layer structure, *J. Appl. Meteor*. **9**, 874-884.

Lenschow, D.H. (1974), Model of the height variation of the turbulence kinetic energy budget in the unstable planetary boundary layer, *J. Atmos. Sci*. **31,** 465-474.

Lenschow, D.H., J.C. Wyngaard, and W.T. Pennell (1980), Mean-field and second-moment budgets in a baroclinic, convective boundary layer, *J. Atmos. Sci*. **37**, 1313-1326.

Lewellen D.C., and W.S. Lewellen (1998), Large-eddy boundary layer entrainment, *J. Atmos. Sci.* **55**, 2645-2665.

Lewellen, D.C., and W.S. Lewellen (2000), Boundary layer entrainment for different capping conditions. **In:** *Proc. 14th Symp. on Boundary Layers and Turbulence, Amer. Meteor. Soc. Aspen, CO*, 80-83.

Lilly, D.K. (1968), Models of cloud-topped mixed layers under a strong inversion, *Quart. J. Roy. Meteor. Soc.* **94,** 292-309.

Mahrt, L., and D.H. Lenschow (1976), Growth dynamics of the convectively mixed layer, *J. Atmos. Sci.* **33**, 41-51.

Margulis, S.A., and D. Entekhabi (2004), Boundary-layer entrainment estimation through assimilation of radiosonde and micrometeorological data into a mixed layer model, *Bound.- Layer Meteor*. **110**, 405-433.

Moeng, C.-H. (1984), A large-eddy simulation for the study of planetary boundary layer turbulence, *J. Atmos. Sci*. **41**, 2052-2062.

Moeng, C.-H., and P.P. Sullivan (1994), A comparison of shear- and buoyancy-driven planetary boundary layer flows, *J. Atmos. Sci*. **51**, 999-1022.

Otte, M.J., and J.C. Wyngaard (2001), Stably stratified interfacial-layer turbulence from large eddy simulation*, J. Atmos. Sci*. **58**, 3424-3442.

Pennel, W.T., and M.A. Lemone (1974), *An experimental study of turbulence in the fair-weather trade wind boundary layer*. J. Atmos. Sci. **31**, 1308-1323.

Pino, D., J.V.-G. de Arellano, and P.J. Duynkerke (2003), The contribution of shear to the evolution of a convective boundary layer, *J. Atmos. Sci*. **60**, 1913-1926.

Pino, D., J.V.-G. de Arellano, and S.-W. Kim (2006), Representing sheared convective boundary layer by zeroth- and first-order-jump mixed-layer models: large-eddy simulation verification, *J. Appl. Meteor. Climatol*. **45,** 1224-1243.

Pope, S.B. (2000), *Turbulent Flows*, Cambridge University Press, Cambridge, 771 pp.

Price, J.F., Mooers, C.N.K., and J.C. Van Leer (1978), Observation and simulation of storm-induced mixed layer deepening, *J. Phys. Oceanogr*. **8**, 582-599.

Randall D.A., and W.H. Schubert (2004), Dreams of a stratocumulus sleeper. **In:** E. Fedorovich *et al*. (eds.), *Atmospheric Turbulence and Mesoscale Meteorology*, Cambridge University Press, Cambridge, 71-94.

Schneider, J.M., and D.K. Lilly (1999), An observational and numerical study of a sheared, convective boundary layer. Part I: Phoenix II observations, statistical description, and visualization, *J. Atmos. Sci*. **56**, 3099-3078.

Sorbjan, Z. (2004), Large-eddy simulation of the baroclinic mixed layer, *Bound.-Layer Meteor*. **112,** 57-80.

Stull, R.B. (1976a), The energetics of entrainment across a density interface, *J. Atmos. Sci*. **33**, 1260-1267.

Stull, R.B. (1976b), Internal gravity waves generated by penetrative convection, *J. Atmos. Sci*. **33**, 1279-1286.

Stull, R.B. (1976c), Mixed-layer depth model based on turbulent energetics, *J. Atmos. Sci*. **33**, 1268-1278.

Stull, R.B. (1988), *An Introduction to Boundary Layer Meteorology*, Kluwer Academic Publishers, Dordrecht, 670 pp.

Sullivan, P., C.-H. Moeng, B. Stevens, D.H. Lenschow, and S.D. Mayor (1998), Structure of the entrainment zone capping the convective atmospheric boundary layer, *J. Atmos. Sci*. **55**, 3042-3064.

Sykes, R.I., and D.S. Henn (1989), Large-eddy simulation of turbulent sheared convection, *J. Atmos. Sci.* **46,** 1106-1118.

Tennekes, H., and A.G.M. Driedonks (1981), Basic entrainment equations for the atmospheric boundary layer, *Bound.-Layer Meteor.* **20,** 515-531.

Xue, M., K.K. Droegemeier, and V. Wong (2000), The advanced regional prediction system (ARPS) – a multi-scale nonhydrostatic atmospheric simulation and prediction model, Part I: Model dynamics and verification, *Meteorol. Atmos. Phys*. **75**, 161-193.

Xue, M., K.K. Droegemeier, V. Wong, A. Shapiro, K. Brewster, F. Carr, D. Weber, Y. Liu, and D. Wang (2001), The advanced regional prediction system (ARPS) – a multi-scale nonhydrostatic atmospheric simulation and prediction model. Part II: Model physics and applications, *Meteorol. Atmos. Phys*. **76**, 143-65.

Zeman, O., and H. Tennekes (1977), Parameterization of the turbulent energy budget at the top of the daytime atmospheric boundary layer, *J. Atmos. Sci*. **34**, 111-123.

Zilitinkevich, S.S. (1991), *Turbulent Penetrative Convection*, Avebury Technical, Aldershot, 179 pp.

Received 13 June 2007
Accepted 6 October 2007